Topology and Geometry of Spin Origami

Krishanu Roychowdhury, D. Zeb Rocklin, and Michael J. Lawler

Phys. Rev. Lett. **121**, 177201 — Published 23 October 2018

DOI: 10.1103/PhysRevLett.121.177201

Topology and geometry of spin origami

Krishanu Roychowdhury,[1,2] D. Zeb Rocklin,[1,3] and Michael J. Lawler[1,2,4]

[1]*Laboratory of Atomic And Solid State Physics, Cornell University, Ithaca, NY 14853.*
[2]*Kavli Institute for Theoretical Physics, University of California, Santa Barbara, CA 93106-4030.*
[3]*School of Physics, Georgia Institute of Technology, Atlanta, GA 30332.*
[4]*Department of Physics, Binghamton University, Binghamton, NY, 13902.*

Kagome antiferromagnets are known to be highly frustrated and degenerate when they possess simple, isotropic interactions. We consider the entire class of these magnets when their interactions are spatially anisotropic. We do so by identifying a certain class of systems whose degenerate ground states can be mapped onto the folding motions of a generalized "spin origami" two-dimensional mechanical sheet. Some such anisotropic spin systems, including $Cs_2ZrCu_3F_{12}$, map onto flat origami sheets, possessing extensive degeneracy similar to isotropic systems. Others, such as $Cs_2CeCu_3F_{12}$, can be mapped onto sheets with non-zero Gaussian curvature, leading to more mechanically stable corrugated surfaces. Remarkably, even such distortions do not always lift the entire degeneracy, instead permitting a large but sub-extensive space of zero-energy modes. We show that for $Cs_2CeCu_3F_{12}$, due to an additional point group symmetry associated with structure, these modes are 'Dirac' line nodes with a double degeneracy protected by a topological invariant. The existence of mechanical analogs thus serves to identify and explicate the robust degeneracy of the spin systems.

Frustrated condensed matter such as kagome Heisenberg antiferromagnets (KHAF) possesses many degenerate ground states that can be either delicate or robust, despite being accidental in the sense of not being protected by a symmetry. Isotropic KHAF have been mapped onto triangulated sheets of "spin origami" [1–3], revealing that, at the classical level, these materials can have as many ground states [4] as there are ways to fold a sheet of paper with one crease for each atomic spin [5]. Splitting this degeneracy by making the magnetic moments spin-$1/2$ would permit the formation of a quantum spin liquid [6, 7], but "clearly the KHAF is a problem where competing states of very different character lie very close in energy" [8]. Like many other strongly correlated materials, a complex phase diagram arises and to our knowledge no general explanation has even been proposed. However, at least in the classical large-S limit, it appears that recent advances in the study of metamaterials [9–20], such as origami, suggest just such an explanation.

Mechanical systems are among the oldest subject to formal study, yet today mechanical metamaterials display new properties and states of matter derived purely from their structure. Many such systems rely on a counting argument developed by Maxwell to determine mechanical stability by counting degrees of freedom (d.o.f.) and constraints [21] and extended by Calladine to account for redundant constraints [22]. Recently, Kane and Lubensky [13] relied on this count to discover, in the context of ball and spring systems, that systems could display exotic zero-energy boundary modes when they had equal numbers of d.o.f. and constraints. In an initially gapped system the difference between these quantities, labeled ν, can only go from 0 to 1, indicating the appearance of a zero mode, when the gap closes. In this context, called "isostatic", ν itself is a topological invariant. Further, they build a local version of Maxwell counting and derive a winding number topological invariant for phonon band structures which demands edge states in "polarized" isostatic systems [13], bulk solitons in isostatic one dimensional systems [23], and Weyl point nodes in isostatic two dimensional systems [18, 24]. In systems with translational symmetries, such a gap trivially closes at wavevector $\mathbf{k} = 0$, but survives for spatially varying modes. Thus, by combining energy gaps with Maxwell counting, a topological mechanics emerges that connects zero modes to topological invariants.

This discovery brings new meaning to Moessner and Chalker's two seminal papers [25, 26] that exploited Maxwell counting to shed light on the accidental ground state degeneracy of classical kagome and a few other antiferromagnets. Grouping the terms in the Hamiltonian into constraints, a procedure that underlies the spin origami construction, they argue Maxwell's ν is often a useful measure of frustration in frustrated magnets. They show that $\nu > 0$ in the pyrochlore Heisenberg antiferromagnet and demands zero modes while ν vanishes in the isotropic kagome KHAF so that its zero modes must arise from a redundancy among the constraints. This redundancy renders the kagome case complex from this perspective, but since it has $\nu = 0$, like Kane and Lubensky's isostatic systems, this complexity should come with topological invariants that could provide an alternative explanation of kagome zero modes.

In this Letter, guided by the concepts of topological mechanics, we study how topology and geometry explicate magnetic frustration in kagome antiferromagnets. Specifically, we solve for the ground states of a class of distorted KHAF obeying a condition (necessary and sufficient) under which the ground states of those systems possess origami analogs. We further identify $Cs_2ZrCu_3F_{12}$ and $Cs_2CeCu_3F_{12}$ as candidate materials that can foster such a spin origami state. Surprisingly, the origami we predict for $Cs_2ZrCu_3F_{12}$ is flattenable like the original spin origami construction of isotropic kagome antiferromagnets despite possessing spatial anisotropies in the spin exchanges. It thus also features a flat band in its spin wave dispersions. In distinction, the origami we find for $Cs_2CeCu_3F_{12}$ is nonflattenable and mechanically more rigid. Nevertheless it retains a finite residual entropy

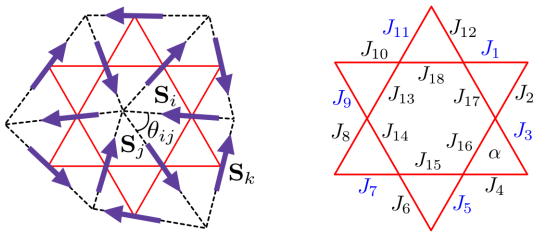

(a) (b)

FIG. 1. (a) Mapping from a spin configuration on the star of David to an origami where the spins in the former represent the edge vectors in the latter drawn in dotted lines. (b) A kagome "Star of David" with nonuniform interactions which on the exterior bonds satisfy the star condition (Eq. 2), necessary for a generic spin system to possess an origami analog. The expression of the interior angle θ_{ij} is given in Eq. (3).

that has dramatic consequences – doubly degenerate topological "Dirac" lines nodes in the spin wave dispersions akin to the Fermi surface of a metal. We discover these lines of zero modes follow from a combination of a special point group symmetry of our predicted nonflattenable periodic origami and a $\mathbb{Z}_2$ topological invariant we build from this symmetry and its isostatic property. In passing, we also find singly degenerate topological "Weyl" lines of zero modes follow from a similar $\mathbb{Z}_2$ topological invariant for generic periodic origami due to their mysterious realness property [20]. Thus, we show these "origami magnets" have robust accidental degeneracy by applying recent developments in the study of metamaterials to that of kagome antiferromagnets.

We define a generic KHAF by [27]

$$\mathcal{H} = \sum_{\langle i,j\rangle} J_{ij}\mathbf{S}_i\cdot\mathbf{S}_j = \frac{1}{2}\sum_{\triangle\alpha,\triangle'\beta} S_{\triangle\alpha}J^{\triangle\alpha,\triangle'\beta}S_{\triangle'\beta} + \text{const.}, \tag{1}$$

where $\alpha \in \{x,y,z\}$ denote the spin components of the spin vector $\mathbf{S}_i$, $J^{\triangle\alpha,\triangle'\beta}$ is a positive definite symmetric matrix, $S_{\triangle\alpha} = \ell_i^{\triangle}S_{i\alpha} + \ell_j^{\triangle}S_{j\alpha} + \ell_k^{\triangle}S_{k\alpha}$ with $\triangle$ denoting a triangle with sites ijk, and $\ell_i^{\triangle}$ are (dimensionless) positive real numbers. This form can be worked out straightforwardly for exclusively nearest neighbor exchanges. The result is $J^{\triangle\alpha,\triangle'\beta} = J_{\triangle}\delta_{\triangle,\triangle'}\delta_{\alpha,\beta}$, $J_{\triangle} > 0$ and $\ell_i^{\triangle} = \sqrt{J_{ij}J_{ik}/J_{\triangle}J_{jk}}$ for triangle $\triangle = \langle ijk\rangle$. The zero-energy condition then requires that the fixed-length vectors $\ell_i^{\triangle}S_{i\alpha}$ on a triangle sum to zero ($S_{\triangle\alpha} = 0$), the very condition that is met by vectors along the edges of a rigid triangle of the type shown in Fig. 1 (a), provided the anisotropy is not so strong that the triangle inequality $\ell_i^{\triangle} < \ell_j^{\triangle} + \ell_k^{\triangle}$ or its cyclic permutations are violated. For the case of isotropic KHAF, these triangles permitted the mapping of zero-energy configurations onto folding patterns of an origami sheet consisting of equilateral triangular faces [1–3, 5].

For an inhomogeneous system, however, we cannot guarantee the existence of an origami analog merely by satisfying $\sum_{\triangle}\ell_i\mathbf{S}_i = 0$. This mapping specifies the shape of the triangular face but not its scale; since each edge corresponds to two faces but can have only one length ($\ell_i^{\triangle} = \ell_i^{\triangle'}$), an additional requirement emerges on the couplings around a magnetic system such as those found in Fig. 1 (b) (see supplementary material):

$$J_1J_3J_5J_7J_9J_{11} = J_2J_4J_6J_8J_{10}J_{12}, \tag{2}$$

where here we explicitly labeled the bonds of the lattice for clarity. As we will see, this condition is met for some but not all KHAF systems. It is a *necessary and sufficient* condition for the existence of a particular (up to overall scale) origami analog that corresponds to the ground state of a generic KHAF (see supplementary material). However, even among such systems, an important distinction arises depending on the geometry of the origami.

Vertices satisfying Eq. (2) are not in general flat. The interior angle of the triangular surface associated with, e.g., the triangle formed by $\mathbf{S}_i$, $\mathbf{S}_j$, and $\mathbf{S}_k$ in Fig. 1 i.e. the angle between $\mathbf{S}_i$ and $\mathbf{S}_j$ is given by

$$\theta_{ij} = \cos^{-1}\left[\frac{1}{2}\left(\frac{J_{ik}}{J_{jk}} + \frac{J_{jk}}{J_{ik}} - \frac{J_{ik}J_{jk}}{J_{ij}^2}\right)\right]. \tag{3}$$

We can compute them directly from the exchange constants. It is only the special case for which the sum over the angles about a vertex is 2π when the vertex can be formed from a flat sheet, the condition that is usually (but not always [28, 29]) assumed for origami. "Non-Euclidean" vertices violate this, and are said to have nonzero discrete Gaussian curvature (they are nonflattenable, as described in the supplementary material [30]) equal to the angle deficit [31]

$$\mathcal{G}_{\hexagon} = 2\pi - \sum_{\langle ij\rangle\in\hexagon}\theta_{ij}, \tag{4}$$

where $\langle ij\rangle \in \hexagon$ denotes all adjacent pairs of spins $\mathbf{S}_i$ and $\mathbf{S}_j$ that meet at the vertex at the center of the hexagon $\hexagon$. When this angle deficit vanishes, the spins adjoining the vertex can be and are expected [32] to be coplanar. In this case, each vertex possesses a zero mode corresponding to rotating the spins (edges) out of plane. In contrast, nonzero angle deficits preclude these local zero modes and necessarily lift the extensive degeneracy. Thus, the sign of each vertex's angle deficit, $\mu_{\hexagon} \equiv \text{sgn}(\mathcal{G}_{\hexagon})$ is a topological invariant, in that it can change only when zero modes appear. More generally, other classes of systems might lack zero modes even when $\mu_{\hexagon} = 0$ because spins are prevented by their neighbors from assuming coplanar configurations.

Note that these angle deficits, like the angles themselves, depend only on the coupling constants [via Eq. (3)] and not on the spin orientations. In the language of differential geometry, this is Gauss's "Theorema Egregium", that the Gaussian curvature is intrinsic to the system and does not depend on changes to its configuration that are isometries (zero modes) [33, 34]. Thus, degeneracy is determined not by fluctuations or dynamics but is largely determined by hidden geometric constraints. While individual vertices are governed by

geometry, they are collectively constrained to have zero total angle deficit, due to *topological* constraints on the curvature given by the Gauss-Bonnet theorem as described in the supplementary material.

Among kagome materials that meet the star condition [Eq. (2)] despite distortion, we identify two that exemplify sharply distinct degeneracy. $Cs_2ZrCu_3F_{12}$ [35, 36] has a pattern of spins shown in Fig. 2 (a) that, despite distortion, nevertheless lead to flat vertices. Hence, they resemble the isotropic spin origami previously studied [1, 2] despite their distortion. In contrast, $Cs_2CeCu_3F_{12}$ [37], as shown in Fig. 2 (b), with vertices having a finite curvature $\pm\mathcal{G}$ with

$$\mathcal{G} = 4\cos^{-1}\frac{J_3}{2J_2} - 4\cos^{-1}\frac{J_4}{2J_1}. \tag{5}$$

Evidently, $\mathcal{G} \leftrightarrow -\mathcal{G}$ when $J_{1,4} \leftrightarrow J_{2,3}$. The experimentally measured values of the interaction parameters $J_1 = 316$ K, $J_2 = 297$ K, $J_3 = 88$ K, and $J_4 = 85$ K (taken from Ref. [37]) yields $\mathcal{G} \sim -0.055$ [Fig. 2 (b)]. Straining the system tunes the interactions away from these values pushing the origami analog through a flat state and should therefore result in a topological phase transition in the sense of altering the invariant $\mu_{\bigcirc} \equiv \mathrm{sgn}(\mathcal{G}_{\bigcirc})$, as described in the supplementary material. Such a situation is experimentally conceivable as a controlled tuning of interactions in kagome systems has been achieved by means of applying pressure [38] or uniaxial stress [39].

Given the ground state ordering patterns of the Fluoride materials shown in Fig. 2, we now turn to the question of whether the associated spin waves in those materials have any special features. We can qualitatively understand the frustration associated with the zero modes of these two materials by borrowing the concept of self stresses from topological mechanics. In the mechanical analog of the flat spin origami sheet (as in $Cs_2ZrCu_3F_{12}$), we can add tensions to the twelve edges of the six triangular faces adjoining a given vertex while preserving mechanical equilibrium regardless of the shapes of the coplanar faces. These self stress modes then imply the existence of zero modes since they correspond to redundancy of constraints functions in the triangle conditions [22]. These zero modes are displacements of vertices in the direction perpendicular to the faces. They are the manifestation in distorted kagome antiferromagnets with flattenable origami ground states of the zero modes existing in isotropic kagome antiferromagnets. However, for generic nonflattenable origami with non-coplanar edges, as in the $Cs_2CeCu_3F_{12}$ compound, many of these self stresses are no longer possible—the rigidity of the sheet has become fundamentally enhanced via its geometry in a process akin to corrugation. This then has the effect of lifting the zero-energy band of phonons (lattice vibrations) from the origami system and magnons from the analogous spin system. The mechanical responses thus predict a flat band of spin waves associated with flattenable origami ground states (frustration preserved by distortions) but dispersing bands for nonflattenable origami and suggests μ, mentioned above, may be a topological invariant whose change is associated with the emergence of a zero mode. So at this level we predict frustration can be relieved by the distortions in $Cs_2CeCu_3F_{12}$ but not in $Cs_2ZrCu_3F_{12}$.

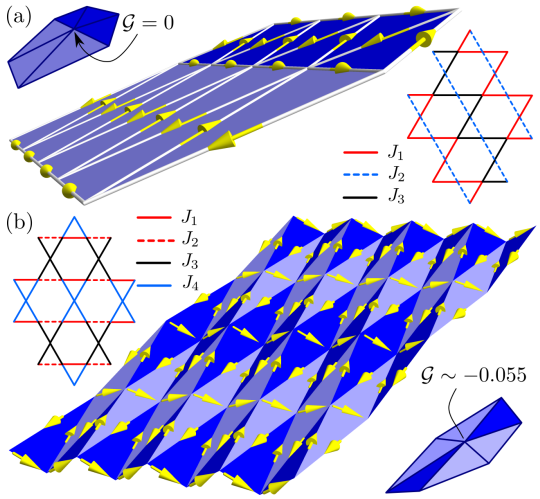

FIG. 2. (a) Right: The distorted kagome lattice structure of $Cs_2ZrCu_3F_{12}$ with interactions that satisfy the star condition. Left: The origami analog of the $q = 0$ state of (a) is a flat sheet ($\mathcal{G} = 0$ at each vertex as shown) consisting of isosceles triangles. The dark blue and the light blue faces correspond respectively to the blue-black and red-blue triangles of the kagome lattice shown in the right. (b) Left: The distorted kagome lattice structure of $Cs_2CeCu_3F_{12}$ with interactions obeying the star condition. Right: The spin origami for a $q = 0$ state is a nonflattenable surface (with finite $\mathcal{G}$ defined in Eq. 5) with coplanar pairs of triangles that form diamond shapes. The spin configurations for both are denoted by yellow arrows.

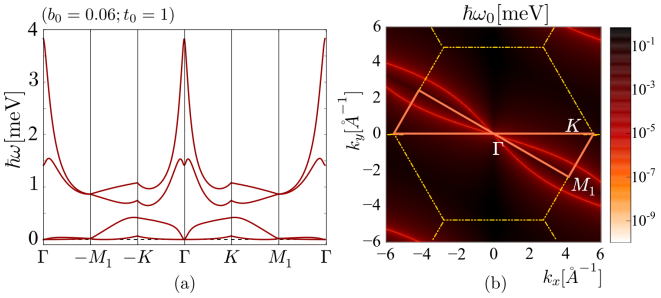

FIG. 3. (a) Some of the lowest spin wave frequencies of $Cs_2CeCu_3F_{12}$ as plotted along the high-symmetry path in the BZ shown in the inset and corresponding to the ground state specified by $b_0 = 0.06$ (see supplementary material for the definition of b_0). (b) A plot (in log scale) of the lowest frequency (ω_0) in the BZ reveals the Dirac Line nodes.

We can learn more about the zero modes by considering the rigidity matrix [13]. It characterizes the entire linear spin-wave theory of spin origami, which we choose to describe in terms of small spin rotations about the ground state using canonical variables $x^{i\mu} \equiv (q^i, p_i)$ (see supplementary material). From the constraint functions of the triangle condition, the rigidity matrix is just the leading term obtained by expand-

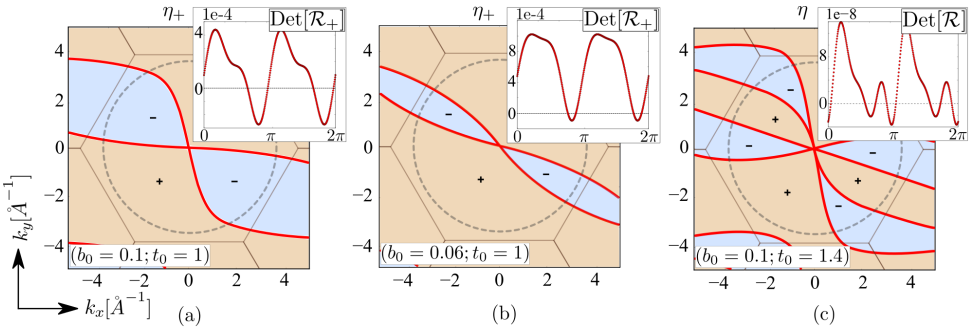

FIG. 4. (a) and (b) Dirac line nodes (thick red lines) separating zones of different values of η_+ (yellow and blue correspond to '+' and '-' respectively) in the spin wave dispersions of $Cs_2CeCu_3F_{12}$. We study these here for two different ground states (defined by the parameter b_0) that represent two members of the one dimensional family of origami configurations obtained for the periodic state (see supplementary material). The insets of (a) and (b) are the plots of η_+ over a circle in the BZ shown on the dotted line. The locations of the lines are decided by the condition $\text{Det}[\mathcal{R}(\mathbf{k})] = 0$ and depend on b_0. (c) Under deformations that break the point group symmetry of $Cs_2CeCu_3F_{12}$, each Dirac line splits into two Weyl lines which are characterized by η in Eq. 8. The inset of (c) is the plot of η over a circle in the BZ.

ing in $x^{i\mu}$ [27]:

$$\mathcal{R}_{\Delta\alpha,i\mu} = \frac{\partial S_{\Delta\alpha}}{\partial x^{i\mu}}. \tag{6}$$

The Hamiltonian matrix governing the spin waves is then $\mathcal{H}_{\text{SW}} = \mathcal{R}^T\mathcal{R}$ where $\mathcal{R}$ is a square matrix because the number of constraints is equal to the number of degrees of freedom $\nu = D - K = 0$. Solving for the spin wave frequencies, we find a flat band for the flattenable origami of $Cs_2ZrCu_3F_{12}$ as expected but doubly degenerate "Dirac" line nodes for $Cs_2CeCu_3F_{12}$ (see Fig. 3). Existence similar line nodes have been previously reported in certain 3D topological semimetals (see Ref. [40] and references therein), however, not in magnetic systems or in 2D. So the rigidity matrix both encodes the flat spin wave band of a flat origami and reveals line nodes of nonflattenable origami.

Zero modes occur precisely at those wavevectors for which $\text{Det}[\mathcal{R}(\mathbf{k})]$ vanishes. This determinant is for general mechanical systems complex, leading to nonzero winding numbers

$$w(C) = \frac{1}{2\pi}\oint_C d(\arg \text{Det}[\mathcal{R}(\mathbf{k})]), \tag{7}$$

around paths C in the Brillouin Zone that are protected under lattice distortions. It either measures the circulation of isolated Weyl point nodes C encloses [18, 24] or characterizes the topological polarization if C is a non-contractible loop across the torus [13]. But remarkably, *for a generic model of spin origami* we find $\text{Det}[\mathcal{R}(\mathbf{k})]$ is a real number up to an overall constant phase in the Brillouin zone (BZ). It obeys the mysterious "realness" condition previously observed for the rigidity matrices of triangulated mechanical origami [20]. The winding numbers $w(C)$ therefore vanish for all C. After eliminating a constant phase by choosing a gauge, however, this realness condition defines another topological number:

$$\eta(\mathbf{k}) = \text{sign Det}[\mathcal{R}(\mathbf{k})]. \tag{8}$$

It demands two regions in the BZ with different $\eta(\mathbf{k})$ are separated by a line of zero modes – the topological Weyl line nodes. We illustrate this in the supplementary material by generating periodic origami and observing how these line nodes move and can vanish pairwise. So just by computing $\eta(\mathbf{k})$ we can learn a lot about the zero modes: while they may be lifted by distortions [see Fig. 4 (c)], a generic nonflattenable origami typically still has topological Weyl line nodes in its spin wave dispersion. The Dirac line nodes must then somehow be pairs of these Weyl line nodes.

To explain the double degeneracy, we have carried out a symmetry analysis in the supplementary material [41]. We now know adding a symmetry can eliminate topology and create new topology. Specifically for $Cs_2CeCu_3F_{12}$, whose triangular faces pair up to create diamond shapes, its point group symmetry explains the numerically observed double degeneracy by playing a role analogous to Kramers degeneracy in a metal. By plotting the 12 spins within the unit cell with tails at a common origin we have uncovered precisely such a symmetry. We find the point group has both unitary and antiunitary symmetries which guarantee that we can place the rigidity matrix in a block diagonal form with two 12×12 blocks each with just real numbers as their elements. The determinant then becomes $\text{Det}[\mathcal{R}(\mathbf{k})] = \text{Det}[\mathcal{R}_+(\mathbf{k})]\text{Det}[\mathcal{R}_-(\mathbf{k})]$ where not only $\text{Det}[\mathcal{R}(\mathbf{k})]$ is real, but also $\text{Det}[\mathcal{R}_\pm(\mathbf{k})]$. We can then define new topological invariants $\eta_\pm(\mathbf{k}) = \text{sign Det}[\mathcal{R}_\pm(\mathbf{k})]$ with $\eta(\mathbf{k}) = \eta_+(\mathbf{k})\eta_-(\mathbf{k})$. A plot of $\eta_+(\mathbf{k})$ is shown in Fig. 4 evincing the effects of distortion that splits the Dirac line nodes into Weyl type. The point group symmetry further demands they both change sign if one of them changes sign so that $\eta(\mathbf{k})$ never changes sign (a loss of topology) and any line nodes are doubly degenerate (a new topology). Hence, by identifying the full point group symmetry and its antiunitary character, we have explained the topological protection of the double degenerate line nodes.

Finally, we should mention the topology of rigidity matrices for origami that we uncover here has recently been extended to a full classification by two of the authors[42].

In summary we have identified broad classes of KHAF, including two experimentally available fluoride compounds,

whose degenerate ground states can be mapped onto the folding motions of origami sheets. The geometry, symmetry and topology of these mechanical analogs explicates how seemingly comparable spin interactions can either preserve or destroy the extensive frustration, or even give rise to novel Dirac line nodes. This mapping extends the original spin origami concept to permit new notions of folding and straining structured mechanical sheets. New results in topological mechanical metamaterials suggest that other magnetic systems may yet realize exotic gapless modes on the boundary and Weyl point nodes in the bulk.

Acknowledgments :- We thank Tom C. Lubensky, James P. Sethna, and Itai Cohen for useful discussion. KR and MJL acknowledge supported in part by the National Science Foundation under Grant No. NSF PHY17-48958. DZR gratefully acknowledge support from the the ICAM postdoctoral fellowship, the Bethe/KIC Fellowship, and the National Science Foundation Grant No. NSF DMR-1308089..

[1] E. Shender, V. Cherepanov, P. Holdsworth, and A. Berlinsky, Physical review letters **70**, 3812 (1993).
[2] P. Chandra, P. Coleman, and I. Ritchey, Journal de Physique I **3**, 591 (1993).
[3] I. Ritchey, P. Chandra, and P. Coleman, Phys. Rev. B **47**, 15342 (1993).
[4] D. A. Huse and A. D. Rutenberg, Physical Review B **45**, 7536 (1992).
[5] M. J. Lawler, New Journal of Physics **15**, 043043 (2013).
[6] S. Yan, D. A. Huse, and S. R. White, Science **332**, 1173 (2011).
[7] A. Seidel, Physical Review B **80**, 165131 (2009).
[8] H.-J. Liao, Z.-Y. Xie, J. Chen, Z.-Y. Liu, H.-D. Xie, R.-Z. Huang, B. Normand, and T. Xiang, Physical review letters **118**, 137202 (2017).
[9] K. Sun, A. Souslov, X. Mao, and T. Lubensky, Proceedings of the National Academy of Sciences **109**, 12369 (2012).
[10] S. Babaee, J. Shim, J. C. Weaver, E. R. Chen, N. Patel, and K. Bertoldi, Advanced Materials **25**, 5044 (2013).
[11] M. Schenk and S. D. Guest, Proceedings of the National Academy of Sciences **110**, 3276 (2013).
[12] Z. Y. Wei, Z. V. Guo, L. Dudte, H. Y. Liang, and L. Mahadevan, Physical review letters **110**, 215501 (2013).
[13] C. Kane and T. Lubensky, Nature Physics **10**, 39 (2014).
[14] S. Shan, S. H. Kang, P. Wang, C. Qu, S. Shian, E. R. Chen, and K. Bertoldi, Advanced Functional Materials **24**, 4935 (2014).
[15] J. Paulose, A. S. Meeussen, and V. Vitelli, Proceedings of the National Academy of Sciences **112**, 7639 (2015).
[16] D. Rocklin, S. Zhou, K. Sun, and X. Mao, arXiv preprint arXiv:1510.06389 (2015).
[17] T. Lubensky, C. Kane, X. Mao, A. Souslov, and K. Sun, Reports on Progress in Physics **78**, 073901 (2015).
[18] D. Z. Rocklin, B. G.-g. Chen, M. Falk, V. Vitelli, and T. Lubensky, Physical review letters **116**, 135503 (2016).
[19] H. Abbaszadeh, A. Souslov, J. Paulose, H. Schomerus, and V. Vitelli, arXiv preprint arXiv:1610.06406 (2016).
[20] B. G.-g. Chen, B. Liu, A. A. Evans, J. Paulose, I. Cohen, V. Vitelli, and C. Santangelo, Physical review letters **116**, 135501 (2016).
[21] J. C. Maxwell, The London, Edinburgh, and Dublin Philosophical Magazine and Journal of Science **27**, 250 (1864).
[22] C. Calladine, International Journal of Solids and Structures **14**, 161 (1978).
[23] B. G.-g. Chen, N. Upadhyaya, and V. Vitelli, Proceedings of the National Academy of Sciences **111**, 13004 (2014).
[24] H. C. Po, Y. Bahri, and A. Vishwanath, Phys. Rev. B **93**, 205158 (2016).
[25] R. Moessner and J. Chalker, Physical review letters **80**, 2929 (1998).
[26] R. Moessner and J. Chalker, Physical Review B **58**, 12049 (1998).
[27] M. J. Lawler, Physical Review B **94**, 165101 (2016).
[28] J. M. XuehouTan, *Discrete and Computational Geometry* (Springer, 2005).
[29] C. D. Santangelo, Annual Review of Condensed Matter Physics **8**, 165 (2017).
[30] Note Ref. [43, 44] discussing the discrete Gaussian curvature to characterize a nonflattenable surface.
[31] M. Meyer, M. Desbrun, P. Schröder, and A. H. Barr, in *Visualization and mathematics III* (Springer, 2003) pp. 35–57.
[32] A. Chubukov, Physical review letters **69**, 832 (1992).
[33] K. F. Gauss, *General Investigations of Curved Surfaces: Edited with an Introduction and Notes by Peter Pesic* (Courier Corporation, 2013).
[34] K. Tapp, *Differential Geometry of curves and surfaces* (Springer, 2016).
[35] T. Ono, K. Morita, M. Yano, H. Tanaka, K. Fujii, H. Uekusa, Y. Narumi, and K. Kindo, Physical Review B **79**, 174407 (2009).
[36] L. J. Downie, C. Black, E. Ardashnikova, C. Tang, A. Vasiliev, A. Golovanov, P. Berdonosov, V. Dolgikh, and P. Lightfoot, CrystEngComm **16**, 7419 (2014).
[37] T. Amemiya, M. Yano, K. Morita, I. Umegaki, T. Ono, H. Tanaka, K. Fujii, and H. Uekusa, Physical Review B **80**, 100406 (2009).
[38] J. Wang, Y. Feng, R. Jaramillo, J. van Wezel, P. C. Canfield, and T. Rosenbaum, Physical Review B **86**, 014422 (2012).
[39] R. Küchler, C. Stingl, Y. Tokiwa, M. Kim, T. Takabatake, and P. Gegenwart, Physical Review B **96**, 241110 (2017).
[40] Y. Kim, B. J. Wieder, C. Kane, and A. M. Rappe, Physical review letters **115**, 036806 (2015).
[41] Note Ref. [45, 46] for the details of the symmetry implementation.
[42] K. Roychowdhury and M. J. Lawler, Physical Review B **98**, 094432 (2018).
[43] R. D. Kamien, Reviews of Modern physics **74**, 953 (2002).
[44] C. R. Calladine, *Theory of shell structures* (Cambridge University Press, 1988).
[45] E. P. Wigner, Journal of Mathematical Physics **1**, 409 (1960).
[46] A. A. Soluyanov and D. Vanderbilt, Physical Review B **85**, 115415 (2012).